Cumulant expansion approach to the decay dynamics of interacting Mössbauer nuclei after strong impulsive excitation

Miriam Gerharz and Jörg Evers Max-Planck-Institut für Kernphysik, Saupfercheckweg 1, 69117 Heidelberg, Germany

Recent progress in accelerator-based x-ray sources brings higher excitation of ensembles of Mössbauer nuclei closer to experimental feasibility. Yet, a theoretical modeling of the decay dynamics of the interacting nuclear ensemble after the impulsive excitation is still an open challenge. Here, we derive a set of nonlinear equations which is capable of efficiently modeling large nuclear ensembles for arbitrary degrees of excitation. As key signature for higher excitation, we identify a non-linear time-evolution of the nuclear dipole phase, which can be tuned via the scattering geometry, and interferometrically be measured. Furthermore, we identify interesting finite-size effects in the nuclear dynamics of small ensembles. Our results provide important guidance for future experiments aiming at the non-linear excitation of nuclei. We further envision the exploration of finite size-effects in Mössbauer spectroscopy with highest spatial resolution, i.e., small sample volumes.

Mössbauer nuclei have already proven to be a versatile platform for quantum optics and related concepts, even though typical experiments so far have been restricted to the low-excitation limit with less than one signal photon on average due to source limitations [1-24]. X-ray freeelectron lasers [25–33] provide access to new excitation regimes which are expected to advance the field [13, 34], and first experiments have already demonstrated some of the novel possibilities [35–38]. Towards higher excitation, more than 900 signal photons after a single x-ray excitation have been observed recently [38], and it has been theoretically proposed that focusing the x-ray beam could significantly enhance the fraction of excited nuclei in the ensemble [39]. Further source development such as x-ray free-electron laser oscillators [40–42] could even bring full inversion of an ensemble of Mössbauer nuclei within reach [39, 43].

A corresponding theoretical framework is therefore required to match the pace of experimental advances. From a theoretical point of view, the nuclear ensemble forms an interacting many-body system. As such, the problem is strongly related to other many-body systems from a theoretical point of view. A particular challenge is that in general the interaction between the nuclei and the incoherent loss channels may operate on comparable time scales, such that neither dominates. This renders some of the well-known approaches less suitable (see, e.g., the discussion in [44]). In the low-excitation limit, the resulting equations can analytically be solved, giving rise, e.g., to the well-known response function formalism [45, 46] and quantum optical models [47–49]. Towards higher excitation, different theoretical approaches have been pursued. Typical experiments excite the nuclei impulsively, fast as compared to all other time scales in the system. This allows one to separate and analytically solve the nuclear excitation [39, 50]. By contrast, the subsequent decay dynamics of the interacting ensemble of nuclei is much harder to treat. It has been suggested to use a perturbative approach to characterize the nuclear dynamics in leading order beyond the linear case [51]. This approach allows one to derive experimental signatures for the non-linear excitation, but it fails towards higher excitation. Assuming that the dynamics is restricted to the fully symmetric superradiant subspace, the dynamics can also be evaluated [52]. However, this approach fails to capture the incoherent single-particle dynamics which evolves the system out of the symmetric subspace, but is crucial in nuclei due to the non-radiative internal conversion channel [46, 53]. Recently, it has been suggested to use a matrix-product state approach [54] to model the many-body dynamics [55]. This approach can handle higher excitation and allows one to analyze photon correlations, but only a small number of nuclei can be modeled without further approximations and entanglement between the particles is only partially captured.

In the following, we pursue a different approach, which exploits that in typical bulk target materials the coupling between the nuclei is moderate. This suggests a perturbative expansion in the nuclear coupling, rather than an expansion in the degree of excitation or a truncation of the Hilbert space. One approach is the *cumulant expansion* [56], which is well-known in modeling many-body dynamics in general [57–62] but so far has not been applied to model the dynamics of Mössbauer nuclei.

Here, we solve the nuclear many-body system using a cumulant expansion approach. We derive effective manybody equations valid for arbitrary degrees of excitation. which can efficiently be solved even for larger ensembles since their number scales linearly with that of the nuclei. Assuming further a translational invariance in an extended ensemble under homogeneous excitation conditions, we derive an effective single-particle non-linear equation of motion which captures the many-body dynamics in leading order of the cumulant expansion. It allows one to model the many-body system very efficiently, independent of the number of nuclei. Solving this equation, we show that towards higher excitation, the couplings between the nuclei imply a characteristic non-linear evolution of the nuclear dipole phase, and put forward a method to interferometrically measure it which

exploits the geometry-dependence of the inter-nuclear couplings. By comparing with the case without translational invariance, we further uncover interesting finitesize effects in smaller ensembles which could also be experimentally explored.

Decay dynamics of the nuclear many-body system. The decay dynamics can be modeled using a master equation for N nuclei [47, 63–65]

$$\dot{\rho} = \frac{1}{i\hbar} \left[H, \rho \right] + \mathcal{L}[\rho] \tag{1}$$

$$H = -\hbar \sum_{n m=1}^{N} J_{mn} \, \sigma_n^+ \, \sigma_m^-,$$
 (2)

$$\mathcal{L}[\rho] = \sum_{n,m=1}^{N} \frac{\Gamma_{mn}}{2} \left(2\sigma_{m}^{-} \rho \sigma_{n}^{+} - \sigma_{n}^{+} \sigma_{m}^{-} \rho - \rho \sigma_{n}^{+} \sigma_{m}^{-} \right) , \quad (3)$$

where $\Gamma_{mn} = \Gamma_{mn}^{\rm rad} + \delta_{mn} \Gamma^{\rm IC}$. Here, $\mathcal{L}[\rho]$ describes the incoherent dynamics, where $\Gamma = \Gamma_{nn}$ is the single-particle total decay rate ($\Gamma = 4.7 \,\mathrm{neV}$ for the ⁵⁷Fe Mössbauer transition at 14.4 keV) comprising a radiative ($\Gamma_{nn}^{\rm rad}$) and a non-radiative ($\Gamma^{\rm IC}$) contribution. The other elements J_{nm} and $\Gamma_{nm}^{\rm rad}$ with $n \neq m$ describe the coherent and the incoherent coupling rates between two nuclei n, m which are derived by tracing out the modes of the environmental radiation field.

We proceed by deriving equations of motion for the expectation values of relevant single-particle operators σ_l^- and $\sigma_l^{ee} = \sigma_l^+ \sigma_l^-$, where the former characterizes the coherence and the latter the excited-state population of atom l. Here, σ_l^{\pm} are Pauli raising and lowering spin operators acting on atom l. We obtain

$$\begin{split} \frac{d}{dt} \langle \sigma_l^- \rangle &= -\frac{\Gamma_{ll}}{2} \left\langle \sigma_l^- \right\rangle \\ &- \sum_{\substack{n=1\\n \neq l}}^N \mathcal{C}_{nl}^* \left(\left\langle \sigma_n^- \right\rangle - 2 \left\langle \sigma_l^{ee} \sigma_n^- \right\rangle \right) \,, \end{split} \tag{4}$$

$$\frac{d}{dt} \langle \sigma_l^{ee} \rangle = -\Gamma_{ll} \langle \sigma_l^{ee} \rangle
- \sum_{\substack{n=1\\n \neq l}}^{N} \mathcal{C}_{nl} \langle \sigma_n^+ \sigma_l^- \rangle + \mathcal{C}_{ln}^* \langle \sigma_l^+ \sigma_n^- \rangle , \quad (5)$$

where $C_{mn} = \frac{\Gamma_{mn}}{2} + iJ_{mn}$.

Cumulant expansion. The equations of motion for the single-particle expectation values Eqs. (4) and (5) depend on two-particle expectation values. This hierarchy generalizes to higher-order expectation values, rendering an exact solution impossible. In the cumulant expansion approach, a closed set of equations is obtained by truncating this hierarchy at a given order [56]. We employ the first order expansion, by approximating

$$\langle A_n B_m \rangle \approx \langle A_n \rangle \langle B_m \rangle \qquad (n \neq m),$$
 (6)

for operators acting on different atoms $n \neq m$. We obtain

$$\frac{d}{dt}\langle\bar{\sigma}_{l}^{-}\rangle = -\frac{\Gamma_{ll}}{2}\left\langle\bar{\sigma}_{l}^{-}\right\rangle - \left(1 - 2\left\langle\sigma_{l}^{ee}\right\rangle\right)\kappa_{l}^{R},\tag{7}$$

$$\frac{d}{dt}\phi_l = -\left(1 - 2\left\langle\sigma_l^{ee}\right\rangle\right)\left\langle\bar{\sigma}_l^-\right\rangle^{-1}\kappa_l^I,\tag{8}$$

$$\frac{d}{dt}\langle \sigma_l^{ee} \rangle = -\Gamma_{ll}\langle \sigma_l^{ee} \rangle - 2 \langle \bar{\sigma}_l^- \rangle \kappa_l^R, \qquad (9)$$

$$\kappa_l = \kappa_l^R + i\kappa_l^I = \sum_{\substack{n=1\\n\neq l}}^N \mathcal{C}_{nl}^* \langle \bar{\sigma}_n^- \rangle e^{i(\phi_n - \phi_l)} \,. \tag{10}$$

Here, we have further decomposed the nuclear coherences into their magnitude and their phase, $\langle \sigma_l^- \rangle = |\langle \sigma_l^- \rangle| \, e^{i\phi_l} = \langle \bar{\sigma}_l^- \rangle \, e^{i\phi_l}$. We find from Eq. (8) that the phase ϕ_l of the nuclear dipole moments in general has a non-linear and excitation-dependent time evolution. Below we develop this feature as a signature for non-linear nuclear excitation.

Note that the Eqs. (7)-(9) already admit for an efficient numerical simulation, since they have a favorable linear scaling with the number of nuclei N. In contrast, the number of matrix elements of the original density operator scales exponentially with N.

Translationally invariant systems. We now continue the discussion by focusing on translationally invariant systems, which will allow us to reduce the computational effort further. To this end, we assume that the nuclei are arranged in an infinite translationally invariant lattice. Furthermore, we assume that the initial excitation is due to a plane wave field incident with wave vector \vec{k} on all nuclei with the same magnitude. Hence, the coherences of all nuclei after the excitation differ only in their initial phases $\phi_l(0)$. In this case, Eqs. (7)-(9) become

$$\frac{d}{dt}\langle \bar{\sigma}^{-}\rangle = -\frac{\Gamma}{2} \left\langle \bar{\sigma}^{-}\right\rangle - (1 - 2 \left\langle \sigma^{ee}\right\rangle) \left\langle \bar{\sigma}^{-}\right\rangle K^{R}, \quad (11)$$

$$\frac{d}{dt}\phi = -\left(1 - 2\left\langle\sigma^{ee}\right\rangle\right)K^{I},\tag{12}$$

$$\frac{d}{dt}\langle\sigma^{ee}\rangle = -\Gamma\langle\sigma^{ee}\rangle - 2\langle\bar{\sigma}^{-}\rangle K^{R}, \qquad (13)$$

$$K = K_l = \sum_{\substack{n=1\\n\neq l}}^{N} \mathcal{C}_{nl}^* e^{i(\phi_n(0) - \phi_l(0))}.$$
 (14)

Here, $\langle \bar{\sigma}^- \rangle = \langle \bar{\sigma}_l^- \rangle$, $\langle \bar{\sigma}^{ee} \rangle = \langle \bar{\sigma}_l^{ee} \rangle$ and $K = K_l$ are the same for all atoms, respectively, and K^R and K^I denote the real and imaginary part of K, respectively. Analogously, the nuclear phase evolves as $\phi_l = \phi_l(0) + \phi$ including the initial excitation phase. Finally, K is a constant which crucially determines the dynamics.

As a result we find that for typical experimental situations, the many-body dynamics can be modeled using a simple set of nonlinear equations, independent of the number of nuclei. In the Appendix, a comparison to chains of finite length is provided, which supports the validity of our translationally invariant model.

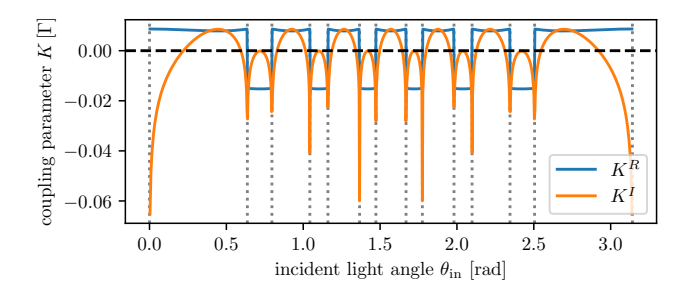


FIG. 1. Coupling parameter $K = K^R + iK^I$ as function of the incident angle $\theta_{\rm in}$. For the calculation, Eq. (16) is used with dipole orientation $\theta_d = \pi/2$.

Temporal dynamics in the low-excitation limit. Eqs. (11)-(13) immediately allow us to connect our results to known phenomena in the well-studied low-excitation limit $\rho^{ee} \approx 0$. Then, the equations of motion reduce to $\frac{d}{dt} \langle \bar{\sigma}^- \rangle \approx -(\Gamma/2 + K^R) \langle \bar{\sigma}^- \rangle$ and $\frac{d}{dt} \phi \approx -K^I$. From these equations we can immediately interpret the real and imaginary parts of K in terms of a superradiant broadening and an interaction-induced energy shift of the nuclear resonance, respectively [1, 13, 46].

Temporal dynamics beyond the low-excitation limit. Next we turn to the largely unexplored regime of higher excitation. We start by noting that the magnitude of the coupling parameter K generally is small as compared to Γ . The reason is that the total decay rate Γ is dominated by the non-radiative (internal conversion) parts $\Gamma^{\rm IC}$ which do not contribute to the couplings (a more detailed numerical study of K is provided below). Therefore the phase of the nuclear dipole moment Eq. (11) is the most promising signature for effects of the non-linear excitation, as it is only governed by K, but not by Γ . In order to derive its time evolution, we can approximately solve for $\langle \sigma^{ee} \rangle$ by neglecting the small contribution K^R in Eq. (13). Inserting the solution $\langle \sigma^{ee} \rangle(t) \approx \sin^2(A/2) \exp(-\Gamma t)$ into Eq. (11), we find

$$\phi(t) = -K^{I} \left[t - \frac{2}{\Gamma} \left(1 - e^{-\Gamma t} \right) \sin^{2} \left(\frac{\mathcal{A}}{2} \right) \right] + \phi_{0} . \quad (15)$$

Here, \mathcal{A} is the pulse area characterizing the initial nuclear excitation via $\langle \sigma^{ee} \rangle(0) = \sin^2(\mathcal{A}/2)$ and $\langle \bar{\sigma}^- \rangle(0) = \sin(\mathcal{A}/2)\cos(\mathcal{A}/2)$ [66]. We find that the nuclear phase evolves non-linearly at intermediate times until $\langle \sigma^{ee} \rangle$ has decayed to zero, with magnitude governed by K^I .

Coupling parameter K. In order to explore the range of the central quantity governing the coupled decay K, we assume that the nuclear dipole moments are aligned at an angle θ_d relative to the chain axis, and that the incident plane wave x-ray pulse propagates at an angle $\theta_{\rm in}$ with respect to the chain. We model the couplings using free-space dipole-dipole couplings [64, 65]. Then,

K becomes (see Appendix)

$$K = -\frac{3i\gamma_0}{2\eta_0} \sin^2(\theta_d) \, \mathcal{X}_1 - \frac{3\gamma_0}{4\eta_0^2} [1 + 3\cos(2\theta_d)] \, \mathcal{X}_2 - \frac{3i\gamma_0}{4\eta_0^3} [1 + 3\cos(2\theta_d)] \, \mathcal{X}_3 \,, \tag{16}$$

where $\mathcal{X}_n = \operatorname{Li}_n(\exp[i(\eta_0 + \Delta\phi)]) + \operatorname{Li}_n(\exp[i(\eta_0 - \Delta\phi)])$ with the polylogarithm $\operatorname{Li}_n(z)$. For the analysis, we use the scaled distance parameter $\eta_0 = k_0 a_0 \approx 21$ with wavevector $k_0 = 2\pi/\lambda_0$ and parameters for ⁵⁷Fe $(\lambda_0 = 86 \text{ pm})$ with nearest-neighbor spacing as in α -Fe $(a_0 = 287 \text{ pm})$. Further $\Delta\phi = \eta_0 \cos\theta_{\rm in}$ characterizes the incident phase difference between two neighboring nuclei.

Results are shown in Fig. 1 as function of the x-ray incidence angle. We use an alignment of the dipole moments $\theta_d = \pi/2$ because in this case the dominant $1/\eta$ -term in K is maximized. Overall, we find that K is comparably small on the scale of the total decay rate Γ , confirming our approximation leading to Eq. (15). For K^{I} , in the center around the perpendicular incident direction, a set of characteristic minima appears. Mathematically these can be traced back to formal divergencies of the polylogarithm for $\theta_d \neq 0$ and $\eta_0 \pm \Delta \phi = n2\pi$ with n an integer. In practice, this divergence is regularized by a finite interaction volume, e.g., limited by the photo-absorption in the target. From an experimental point of view, the region of small incidence angles appears most favorable, since it enables tuning of K^I over its entire range. Small incidence angles also allow for a large number of nuclei in the excitation volume, as required by assumption of translational invariance. For example, a beam of width $100 \,\mu\mathrm{m}$ incident on the chain under an incident light angle of 5 mrad couples to approximately 100 million nuclei.

Numerical simulation of the phase evolution. Finally we turn to a numerical simulation of the phase evolution governed by Eqs. (11)-(13). The result is shown in Fig. 2 for different degrees of initial excitations A and x-ray incidence angles $\theta_{\rm in}$. The blue curves correspond to the limit of linear excitation ($A = 10^{-5}\pi$), with a linear time evolution as expected. From the dotted and the dashed lines we further find that the slope of the phase can be controlled via the incidence angle $\theta_{\rm in}$, as described by K^{I} . Next, we turn to the main results beyond the linear excitation regime. The solid lines of different color show the evolution for different initial degrees of excitation \mathcal{A} at x-ray incidence angle $\theta_{\rm in} = 5\,\mathrm{mrad}$. With increasing excitation, a non-linear time evolution of the phase develops, which leads to a growing deviation from the low-excitation case. At later times, the phase evolution becomes linear again, but an excitation-dependent offset to the linear case remains.

In order to quantify the impact of the assumption of an infinite chain of atoms, the shaded colored lines display the phase evolution of the central atom in a finite chain of $N\,=\,3000$ nuclei. The results qualitatively

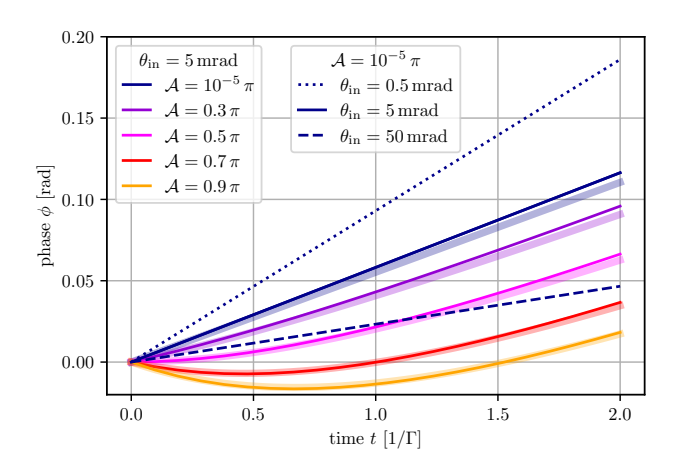


FIG. 2. Nuclear dipole phase evolution as function of incidence angle and degree of excitation. For a fixed incident angle $\theta_{\rm in}=5\,\rm mrad$ the different colors of the solid lines indicate different degrees of initial excitation \mathcal{A} . The transition to a non-linear phase evolution is clearly visible. For comparison, the shaded lines show the results for the central nucleus calculated on a finite chain with N=3000 nuclei. In addition, in the low-excitation regime $\mathcal{A}=10^{-5}\pi$, the different line styles of the blue lines show the results for different incident light angles $\theta_{\rm in}$. The dipole moment is set perpendicular to the chain of nuclei ($\theta_d=\pi/2$).

agree well with the infinite chain results. As discussed in the Appendix, the small quantitative differences can be attributed to the deviation of the finite-chain coupling parameter K to that of the infinite chain, which provide a handle to experimentally explore finite-size effects in nuclear ensembles. We further compare our results to calculations based on the discrete-continuous truncated Wigner approach [44], an alternative approximation which is expected to work best in the case of strong nuclear correlations. We find good qualitative agreement, which supports the validity of the cluster expansion approach for the considered settings.

Experimental signatures of the non-linear phase evolution. Finally we discuss how the non-linear phase evolution shown in Fig. 2 can be experimentally explored. We focus on the scattered electric field, which is commonly observed in experiments with Mössbauer nuclei. The overall electric field is obtained from a suitable summation of the contributions of each of the nuclear dipole moments $\langle \sigma_l^- \rangle$. We consider a scattering geometry in which the differences between the initial phases $\phi_l(0)$ are compensated for by the respective propagational phases from the individual nuclei to the detector, e.g., the forward scattering geometry. In this case, the residual relevant phase evolution of all nuclei is given by $\phi(t)$.

We propose to measure the time evolution of the phase $\phi(t)$ interferometrically, using two chains of nuclei. The orientation of the first chain relative to the x-ray incidence direction is varied, leading to phase evolutions as

shown in Fig. 2. The other reference chain is fixed at an incidence angle where $K^I \approx 0 \ (\theta_{\rm in} \approx 0.22 \, {\rm rad})$. In this setting, the intensity of the x-ray scattered by both chains increases together with the degree of excitation, but only the first one exhibits a non-linear phase evolution, which is ideal for interferometry with high visibility. The effect of the different phase evolutions can then most straightforwardly be measured by detuning the resonance energy of the reference sample by an energy shift Δ , e.g., via a Mössbauer drive [67]. The total intensity then takes the form $I_{\text{comb}}(t) \propto |A_{\text{ref}}(t)e^{i\Delta \cdot t} + A_{\text{sample}}e^{i\phi_{\text{sample}}(t)}|^2$, where $A_{\rm ref}$ and $A_{\rm sample}$ are the amplitudes of the scattered fields of the reference chain and the sample chain, respectively. Assuming that both amplitudes approximately follow the single-particle exponential decay $A_{\rm ref}(t) \approx A_{\rm sample}(t) \approx$ $\exp(-\Gamma t/2)$, the total intensity approximately becomes $I_{\text{comb}} \propto e^{-\Gamma t} \sin[\Delta \cdot t + \phi_{\text{sample}}(t)]$. Hence, the interference between the chains leads to a modulation of the exponentially decaying intensity with frequency Δ . The non-linear phase shift of the first chain shifts this entire quantum beat pattern, facilitating its measurement.

An example for the time-dependent intensity in this detection scheme is shown in Fig. 3. The detuning is chosen as $\Delta = -3\Gamma$. The linear low-excitation case is given by the dark blue line with lowest value for \mathcal{A} . With increasing degree of excitation, the quantum beam minimum progressively shifts towards lower times by a few nanoseconds. Note that state-of-the-art experiments on nuclear forward scattering routinely measure the time-dependence with (sub-)nanosecond resolution. Alternatively, the nuclear phase variation could also be observed via the spectrum of the scattered light, in which already static phase shifts in the low-excitation regime are reflected in the observed line shape [4].

Motivated by recent experimental Discussion. progress, we analyzed the decay dynamics of an interacting ensemble of Mössbauer nuclei after an impulsive excitation by an accelerator-based x-ray source. Unlike previous approaches, we expanded the equations of motion to leading order in the degree of interaction-induced nuclear correlations, which is justified by the comparably small coupling of nuclei in bulk material. Within this approach, we derived equations of motions for the ensemble which scale only linearly in the number of nuclei, and therefore can efficiently be simulated even for larger ensembles. Assuming further a translational invariance of the arrangement of the nuclei and the x-ray excitation, which is a good approximation for established experimental settings, we could further reduce the theoretical description to three non-linear real-valued equations which describe the dynamics of the entire ensemble. We found that the dynamics then is governed by a single coupling parameter K, which can be tuned in experiments.

As the main signature for higher excitation, we found that the inter-nuclear interactions lead to additional non-linear phase dynamics of the nuclear dipole mo-

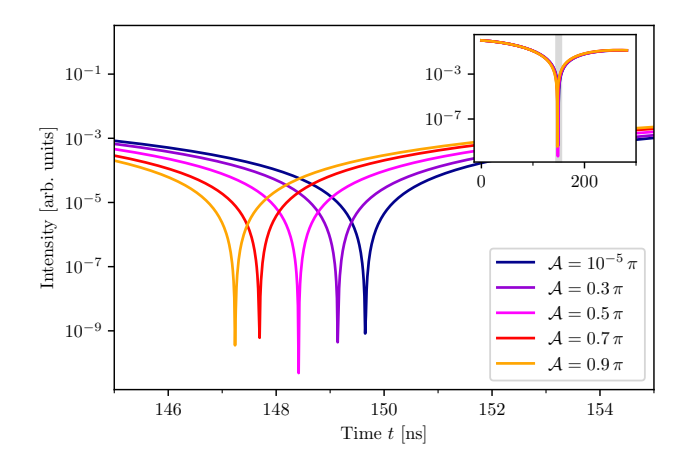


FIG. 3. Time-dependent intensity of the x-ray scattered by two nuclear chains. The reference chain has a detuning of the nuclear resonance of $\Delta=-3\Gamma$., such that the interference between the chains leads to pronounced minima in the intensity. The non-linear phase evolution can then be observed via shifts of these minima in time. The different lines illustrate the dependence on the different degrees of excitation \mathcal{A} . For the sample chain the dipole moment is set perpendicular to the chain of nuclei ($\theta_d=\pi/2$) and the x-ray incidence angles for the sample [reference] chain is 5 mrad [0.22 rad]. The inset shows the signal intensity as a function of time over a larger time interval. The gray area marks the time region shown in the main panel.

ments. Based on this observation, we proposed a setup for measuring this signature, exploiting the geometry-dependence of K. This opens up an approach for the exploration of the non-linear nuclear decay dynamics.

For the future, we envision the generalization of our results to structured nuclear environments, which allow one to engineer and enhance the inter-nuclear couplings [13, 22, 68–70]. Such design capabilities could allow one to achieve particular control operations for the nuclear phase, or to also significantly affect the nuclear population dynamics. Furthermore, source development also brings experiments on smaller samples within reach. We identified characteristic finite-size effects which lead to both, variations in the coupling parameter K with chain length, as well as a dependence of the nuclear dynamics on their position within the chain. We envision future experiments exploring these finite-size effects, e.g., exploring the impact of the geometry on the coherence volume responsible for the collective effects observed in nuclear resonance scattering. Such studies would also form an important basis for future Mössbauer experiments with highest spatial resolution, i.e., small sample volumes.

The authors would like to thank D. Lentrodt for valuable discussions.

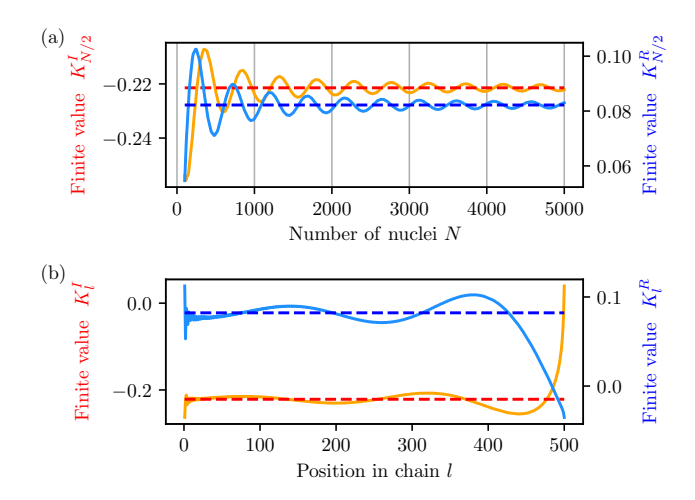


FIG. 4. Comparison of the coupling parameter K_l being evaluated on the finite chain according to Eq. (14) (solid) with that of the infinite chain according to Eq. (16) (dashed). In (a) the coupling parameter K evaluated at the central nucleus l=N/2 is shown as a function of the number of nuclei N. In (b) for a fixed number of nuclei N=500 the coupling parameter is displayed as function of the nucleus' position in the chain l. The calculations are performed for dipole moment perpendicular to the chain $(\theta_d=\pi/2)$ and a small incident light angle of $\theta_{\rm in}=50\,{\rm mrad}$.

Appendix

Finite size effects. In the main text we focus on larger translationally invariant systems, for which we evaluate the coupling parameter K in the limit of an infinite chain Eq. (16). By contrast, for a finite chain of length N, at nucleus l the coupling parameter K_l is given by

$$K_{l} = \sum_{m=1}^{N} C_{lm}^{*} \left(e^{i m \Delta \phi} + e^{-i m \Delta \phi} \right)$$

$$= -3i \gamma_{0} \sum_{m=1}^{\infty} \left[\left(\frac{1}{\eta_{0}m} + \frac{i}{\eta_{0}^{2}m^{2}} - \frac{1}{\eta_{0}^{3}m^{3}} \right) - \cos^{2}(\theta_{d}) \left(\frac{1}{\eta_{0}m} + \frac{3i}{\eta_{0}^{2}m^{2}} - \frac{3}{\eta_{0}^{3}m^{3}} \right) \right] e^{i m \eta_{0}}$$

$$\times \left(e^{i m \Delta \phi} + e^{-i m \Delta \phi} \right). \tag{17}$$

In Fig. 4(a), finite-size effects in the coupling parameter K are explored. It compares the converged K for an infinite chain with the corresponding parameter for the central nucleus l=N/2 in a finite chain of variable length N. Overall, we observe a convergence to the asymptotic value with increasing N. However, the convergence is not monotonic, but governed by oscillations around the asymptotic value with frequency decreasing for smaller incident light angles $\theta_{\rm in}$. The effect of this dependence could be explored in small nuclear ensembles.

Fig. 4(b) shows the coupling parameter for a finite chain K_l in Eq. (14) evaluated as function of the position

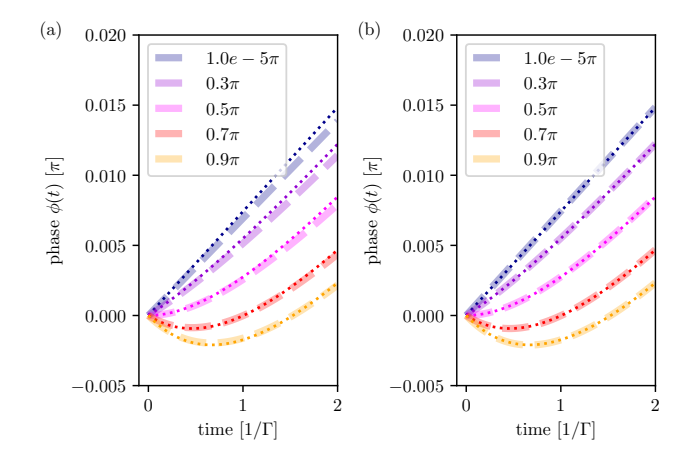


FIG. 5. Comparison of the phase evolution computed with a finite chain evaluated at the central nucleus (dashed) and the translational invariant model (dotted). In (a) the chain has a length of N=362 nuclei, which corresponds to a point of maximal deviation of K in Fig. 4, in (b) a length of N=257 nuclei corresponding to a point of minimal deviation in K is chosen. The different colors indicate different initial excitations \mathcal{A} according to the respective legend. The calculations are performed for dipole moment perpendicular to the chain $(\theta_d=\pi/2)$ and a small incident light angle of $\theta_{\rm in}=50$ mrad.

within the chain l. A pronounced oscillatory dependence on l is clearly visible, depending on the asymmetry in the number of nuclei to the left and right of a certain nucleus l. The oscillations decrease with rising number of nuclei N. However, for smaller chains, they are of relevance in evaluating the far-field scattered electric field, and may modify the angular pattern already in the low-excitation limit [71]. For larger samples, the variations are negligible, which is why we continue with the analysis of finite size effects at the central nucleus only.

To investigate finite size effects during the time evolution, in Fig. 5 the results for the central nucleus in a finite chain (dashed lines) are compared to those from the translational invariant model (dotted lines) for different initial excitations \mathcal{A} . For Fig. 5(a) the number of nuclei is N = 362, which corresponds to a maximal difference of the coupling parameter K^I from the asymptotic value as can be seen from Fig. 4. Although qualitatively the overall trends of the non-linear time-evolution agree for the finite and infinite chain, there are noticeable quantitative differences. In Fig. 5(b) a smaller chain with N=257nuclei, but with minimal deviation of the coupling parameter K^{I} is used. Here, the quantitative agreement is significantly better than in the other case although the chain is smaller. This is already a strong indication, that the dominant finite size effect for observables on the single atom level is the convergence of the coupling parameter K.

To quantify the convergence with chain length, for each observable O we calculate the mean squared absolute dif-

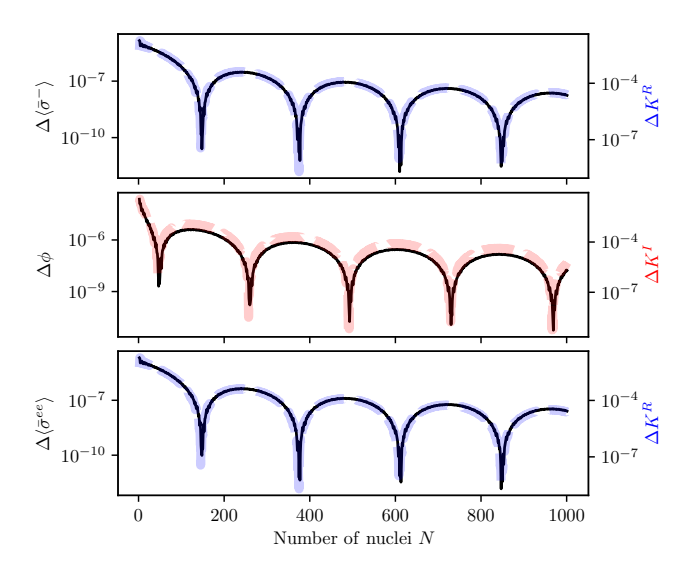


FIG. 6. Impact of finite size effects on the nuclear dynamics. The deviation of observable O is quantified by the integrated quadratic differences over time $\Delta O = \frac{1}{M} \sum_{i=1}^M |O_\infty(t_i)| - O_N(t_i)|^2$, where O_∞ is the result for a translationally invariant infinite chain and O_N is the result from a finite chain of length N evaluated at the central nucleus. The three panels show the deviation as function of chain length N (black markers). The comparison is made for the absolute value of the nuclear coherence (top panel), the phase of the coherence (central panel) and the population (bottom). For comparison, on the second y-axis, the absolute difference $|K_\infty - K_N|$ of the dominant part (real or imaginary part) of the coupling parameter K is shown (red and blue dashed lines). The integration time is up to $t=2/\Gamma$, the dipole is perpendicular to the chain $\theta_d=\pi/2$ and the incident light angle is $\theta_{\rm in}=50$ mrad.

ference between the result from the translational invariant model O_{∞} and the finite chain of length N result O_N integrated over time $\Delta O = \frac{1}{M} \sum_{i=1}^M |O_{\infty}(t_i) - O_N(t_i)|^2$. In Fig. 6 the deviation ΔO is displayed for the absolute value and phase of the coherence and the population evaluated at the central nucleus in the chain l = N/2 as function of the number of nuclei in the chain N. The general trend is that the deviations decrease with rising length of the chain as expected. In addition, the deviations for the absolute values of the coherence and the population are smaller because in the respective equations of motions, the relevant part of the coupling parameter K^R is dominated by the single-particle decay Γ . Besides the general convergence, there is an oscillatory structure. This structure comes from the oscillatory convergence behavior as shown in Fig. 4. To see this more clearly, on a second y-axis for the real and imaginary part, respectively, the squared absolute difference of the coupling parameter calculated for a finite chain K is compared to the asymptotic value given by Eq. 16 is displayed. The oscillatory structure of ΔO clearly follows the differences of K. Therefore, we conclude that for the central nucleus the most-dominant finite size effect is the

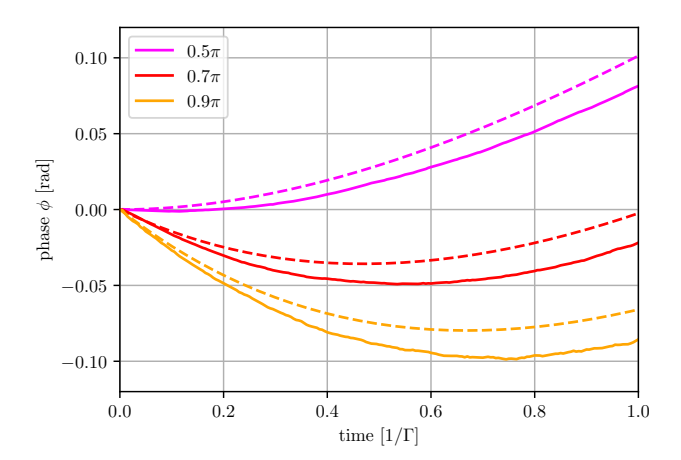


FIG. 7. Phase evolution of the central nucleus in a chain of length N=100. The figure complares results of the cumulant expansion (dashed) with corresponding results obtained from the truncated Wigner approximation (solid). The different colors indicate different initial excitations \mathcal{A} . The calculations are performed without internal conversion ($\Gamma^{\rm IC}=0$) for dipole moment perpendicular to the chain ($\theta_d=\pi/2$) and a small incident light angle of $\theta_{\rm in}=5\,{\rm mrad}$.

difference in the imaginary part of the coupling parameter K^{I} , which in a converging but oscillating manner depends on the number of nuclei in the chain N. Beyond cumulant expansion.

In order to verify that the results discussed in the main text obtained from the cumulant expansion are within the validity range of the method, we compare the results with the phase evolution obtained in the framework of the discrete-continuous truncated Wigner approximation (CDTWA) developed by Mink et al. [44]. This approach is known to work best for stronger couplings and higher excitations, whereas in the opposite case beyond $t = 1/\Gamma$ unphysical effects appear [44]. Therefore, we neglect the internal conversion for this comparison ($\Gamma^{IC} = 0$) which results in higher cooperativity and thus better validity of CDTWA, but is a less favorable parameter range for the cumulant expansion. With internal conversion, the cumulant expansion results are expected to be be more reliable. Nonetheless, the CDTWA provides a good crosscheck for the cumulant expansion results because the approximation methods are complementary to each other. In Fig. 7 for the central nucleus l = N/2 in a chain of length N = 100, the phase evolution calculated with the cumulant expansion and the CDTWA is compared for different initial excitations A. For all three shown different degrees of initial excitation, the results obtained with the cumulant expansion (dashed lines) and CDTWA (solid lines) agree qualitatively well which confirms the non-linear phase evolution.

- R. Röhlsberger, K. Schlage, B. Sahoo, S. Couet, and R. Rüffer, Collective lamb shift in single-photon superradiance, Science 328, 1248 (2010).
- [2] R. Röhlsberger, H.-C. Wille, K. Schlage, and B. Sahoo, Electromagnetically induced transparency with resonant nuclei in a cavity, Nature 482, 199–203 (2012).
- [3] K. P. Heeg, H.-C. Wille, K. Schlage, T. Guryeva, D. Schumacher, I. Uschmann, K. S. Schulze, B. Marx, T. Kämpfer, G. G. Paulus, R. Röhlsberger, and J. Evers, Vacuum-assisted generation and control of atomic coherences at x-ray energies, Phys. Rev. Lett. 111, 073601 (2013).
- [4] K. P. Heeg, C. Ott, D. Schumacher, H.-C. Wille, R. Röhlsberger, T. Pfeifer, and J. Evers, Interferometric phase detection at x-ray energies via Fano resonance control, Phys. Rev. Lett. 114, 207401 (2015).
- [5] K. P. Heeg, J. Haber, D. Schumacher, L. Bocklage, H.-C. Wille, K. S. Schulze, R. Loetzsch, I. Uschmann, G. G. Paulus, R. Rüffer, R. Röhlsberger, and J. Evers, Tunable subluminal propagation of narrow-band x-ray pulses, Phys. Rev. Lett. 114, 203601 (2015).
- [6] J. Haber, K. S. Schulze, K. Schlage, R. Loetzsch, L. Bocklage, T. Gurieva, H. Bernhardt, H.-C. Wille, R. Rüffer, I. Uschmann, G. G. Paulus, and R. Röhlsberger, Collective strong coupling of x-rays and nuclei in a nuclear optical lattice, Nature Photonics 10, 445–449 (2016).
- [7] J. Haber, X. Kong, C. Strohm, S. Willing, J. Gollwitzer, L. Bocklage, R. Rüffer, A. Pálffy, and R. Röhlsberger, Rabi oscillations of x-ray radiation between two nuclear ensembles, Nature Photonics 11, 720–725 (2017).
- [8] X. Zhang, W.-T. Liao, A. Kalachev, R. Shakhmuratov, M. Scully, and O. Kocharovskaya, Nuclear quantum memory and time sequencing of a single γ photon, Phys. Rev. Lett. **123**, 250504 (2019).
- [9] K. P. Heeg, A. Kaldun, C. Strohm, C. Ott, R. Subramanian, D. Lentrodt, J. Haber, H.-C. Wille, S. Goerttler, R. Rüffer, C. H. Keitel, R. Röhlsberger, T. Pfeifer, and J. Evers, Coherent x-ray-optical control of nuclear excitons, Nature 590, 401–404 (2021).
- [10] S. Velten, L. Bocklage, X. Zhang, K. Schlage, A. Panchwanee, S. Sadashivaiah, I. Sergeev, O. Leupold, A. I. Chumakov, O. Kocharovskaya, and R. Röhlsberger, Nuclear quantum memory for hard x-ray photon wave packets, Science Advances 10, eadn9825 (2024).
- [11] Y. V. Shvyd'ko, T. Hertrich, U. van Bürck, E. Gerdau, O. Leupold, J. Metge, H. D. Rüter, S. Schwendy, G. V. Smirnov, W. Potzel, and P. Schindelmann, Storage of nuclear excitation energy through magnetic switching, Phys. Rev. Lett. 77, 3232 (1996).
- [12] P. Helistö, I. Tittonen, M. Lippmaa, and T. Katila, Gamma echo, Phys. Rev. Lett. 66, 2037 (1991).
- [13] R. Röhlsberger and J. Evers, Quantum Optical Phenomena in Nuclear Resonant Scattering, in *Modern Mössbauer Spectroscopy*, Vol. 137, edited by Y. Yoshida and G. Langouche (Springer Singapore, Singapore, 2021) pp. 105–171, series Title: Topics in Applied Physics.
- [14] M. Gerharz, D. Lentrodt, L. Bocklage, K. Schulze, C. Ott, R. Steinbrügge, O. Leupold, I. Sergeev, G. G. Paulus, C. H. Keitel, R. Röhlsberger, T. Pfeifer, and J. Evers, Dark-fringe interferometer with dynamic phase control for Mössbauer science (2025), arXiv:2509.24658

- [quant-ph].
- [15] P. Schindelmann, U. van Bürck, W. Potzel, G. V. Smirnov, S. L. Popov, E. Gerdau, Y. V. Shvyd'ko, J. Jäschke, H. D. Rüter, A. I. Chumakov, and R. Rüffer, Radiative decoupling and coupling of nuclear oscillators by stepwise doppler-energy shifts, Phys. Rev. A 65, 023804 (2002).
- [16] F. Vagizov, V. Antonov, Y. V. Radeonychev, R. N. Shakhmuratov, and O. Kocharovskaya, Coherent control of the waveforms of recoilless γ-ray photons, Nature 508, 80–83 (2014).
- [17] F. G. Vagizov, E. K. Sadykov, and O. A. Kocharovskaya, Modulation of Mössbauer radiation by pulsed laser excitation, JETP Letters 96, 812 (2013).
- [18] S. Sakshath, K. Jenni, L. Scherthan, P. Würtz, M. Herlitschke, I. Sergeev, C. Strohm, H.-C. Wille, R. Röhlsberger, J. A. Wolny, and V. Schünemann, Optical pump - nuclear resonance probe experiments on spin crossover complexes, Hyperfine Interactions 238, 89 (2017).
- [19] E. Kuznetsova, X. Zhang, Y. Shvyd'ko, M. O. Scully, and O. Kocharovskaya, Spectral flux enhancement of x rays for addressing ultranarrow nuclear transitions, Phys. Rev. Lett. 133, 193401 (2024).
- [20] A. Nazeeri, C. Brandenstein, C. Jia, L. Magrini, and G. Gratta, Coupling of a nuclear transition to a surface acoustic wave (2025), arXiv:2509.02750 [quant-ph].
- [21] H. Yamashita, S. Kitao, Y. Kobayashi, and M. Seto, The correlation of the gamma ray waveform with the vibration phase of the resonant absorber, Interactions 245, 10.1007/s10751-024-02214-3 (2024).
- [22] L. M. Lohse, A. Negi, M. Osterhoff, P. Meyer, S. Yaroslavtsev, A. I. Chumakov, L. Bocklage, R. Röhlsberger, and T. Salditt, Interferometric measurement of nuclear resonant phase shift with a nanoscale young double waveguide (2025), arXiv:2506.05823 [physics.optics].
- [23] A. Stejskal, V. Vrba, and V. Procházka, Toward flexible intensity control of resonantly scattered γ -rays using multi-frequency vibrating resonant absorber, Applied Physics Letters **126**, 084102 (2025).
- [24] K. Fujiwara, T. Mitsui, Y. Aoyagi, Y. Yoda, and N. Ikeda, Quantum interference of totally reflected mössbauer γ -rays from a 57fe monolayer embedded in a thin film, Journal of the Physical Society of Japan 90, 084705 (2021).
- [25] P. Emma, R. Akre, J. Arthur, R. Bionta, C. Bostedt, J. Bozek, A. Brachmann, P. Bucksbaum, R. Coffee, F.-J. Decker, Y. Ding, D. Dowell, S. Edstrom, A. Fisher, J. Frisch, S. Gilevich, J. Hastings, G. Hays, P. Hering, Z. Huang, R. Iverson, H. Loos, M. Messerschmidt, A. Miahnahri, S. Moeller, H.-D. Nuhn, G. Pile, D. Ratner, J. Rzepiela, D. Schultz, T. Smith, P. Stefan, H. Tompkins, J. Turner, J. Welch, W. White, J. Wu, G. Yocky, and J. Galayda, First lasing and operation of an angstrom-wavelength free-electron laser, Nature Photonics 4, 641 (2010).
- [26] W. Barletta, J. Bisognano, J. Corlett, P. Emma, Z. Huang, K.-J. Kim, R. Lindberg, J. Murphy, G. Neil, D. Nguyen, C. Pellegrini, R. Rimmer, F. Sannibale, G. Stupakov, R. Walker, and A. Zholents, Free electron lasers: Present status and future challenges, Nuclear Instruments and Methods in Physics Research Section A: Accelerators, Spectrometers, Detectors and Associated

- Equipment 618, 69 (2010).
- [27] T. Ishikawa, H. Aoyagi, T. Asaka, Y. Asano, N. Azumi, T. Bizen, H. Ego, K. Fukami, T. Fukui, Y. Furukawa, S. Goto, H. Hanaki, T. Hara, T. Hasegawa, T. Hatsui, A. Higashiya, T. Hirono, N. Hosoda, M. Ishii, T. Inagaki, Y. Inubushi, T. Itoga, Y. Joti, M. Kago, T. Kameshima, H. Kimura, Y. Kirihara, A. Kiyomichi, T. Kobayashi, C. Kondo, T. Kudo, H. Maesaka, X. M. Maréchal, T. Masuda, S. Matsubara, T. Matsumoto, T. Matsushita, S. Matsui, M. Nagasono, N. Nariyama, H. Ohashi, T. Ohata, T. Ohshima, S. Ono, Y. Otake, C. Saji, T. Sakurai, T. Sato, K. Sawada, T. Seike, K. Shirasawa, T. Sugimoto, S. Suzuki, S. Takahashi, H. Takebe, K. Takeshita, K. Tamasaku, H. Tanaka, R. Tanaka, Tanaka, T. Togashi, K. Togawa, A. Tokuhisa, H. Tomizawa, K. Tono, S. Wu, M. Yabashi, M. Yamaga, A. Yamashita, K. Yanagida, C. Zhang, T. Shintake, H. Kitamura, and N. Kumagai, A compact x-ray freeelectron laser emitting in the sub-ångström region, Nature Photonics **6**, 540 (2012).
- [28] W. Decking, S. Abeghyan, P. Abramian, A. Abramsky, A. Aguirre, C. Albrecht, P. Alou, M. Altarelli, P. Altmann, K. Amyan, et al., A MHz-repetition-rate hard xray free-electron laser driven by a superconducting linear accelerator, Nature photonics 14, 391 (2020).
- [29] J. Amann, W. Berg, V. Blank, F.-J. Decker, Y. Ding, P. Emma, Y. Feng, J. Frisch, D. Fritz, J. Hastings, et al., Demonstration of self-seeding in a hard-x-ray freeelectron laser, Nature photonics 6, 693 (2012).
- [30] I. Inoue, T. Osaka, T. Hara, T. Tanaka, T. Inagaki, T. Fukui, S. Goto, Y. Inubushi, H. Kimura, R. Kinjo, H. Ohashi, K. Togawa, K. Tono, M. Yamaga, H. Tanaka, T. Ishikawa, and M. Yabashi, Generation of narrow-band x-ray free-electron laser via reflection self-seeding, Nature photonics 13, 319 (2019).
- [31] S. Liu, C. Grech, M. Guetg, S. Karabekyan, V. Kocharyan, N. Kujala, C. Lechner, T. Long, N. Mirian, W. Qin, S. Serkez, S. Tomin, J. Yan, S. Abeghyan, J. Anton, V. Blank, U. Boesenberg, F. Brinker, Y. Chen, W. Decking, X. Dong, S. Kearney, D. La Civita, A. Madsen, T. Maltezopoulos, A. Rodriguez-Fernandez, E. Saldin, L. Samoylova, M. Scholz, H. Sinn, V. Sleziona, D. Shu, T. Tanikawa, S. Terentiev, A. Trebushinin, T. Tschentscher, M. Vannoni, T. Wohlenberg, M. Yakopov, and G. Geloni, Cascaded hard x-ray self-seeded free-electron laser at megahertz repetition rate, Nature Photonics 17, 984 (2023).
- [32] I. Nam, C.-K. Min, B. Oh, G. Kim, D. Na, Y. J. Suh, H. Yang, M. H. Cho, C. Kim, M.-J. Kim, C. H. Shim, J. H. Ko, H. Heo, J. Park, J. Kim, S. Park, G. Park, S. Kim, S. H. Chun, H. Hyun, J. H. Lee, K. S. Kim, I. Eom, S. Rah, D. Shu, K.-J. Kim, S. Terentyev, V. Blank, Y. Shvyd'ko, S. J. Lee, and H.-S. Kang, Highbrightness self-seeded x-ray free-electron laser covering the 3.5 keV to 14.6 keV range, Nature Photonics 15, 435 (2021).
- [33] S. Liu, G. Geloni, T. Long, W. Qin, V. Kocharyan, J. Yan, L. Cao, N. Kujala, M. Guetg, M. Scholz, and W. Decking, Updates on the hard x-ray self-seeding at the european xfel, Synchrotron Radiation News 38, 11 (2025).
- [34] G. Shenoy, Dreams with synchrotron radiation, in The Rudolf Mössbauer Story: His Scientific Work and Its Impact on Science and History, edited by G. Kalvius and

- P. Kienle (Springer, Berlin, Heidelberg, 2012).
- [35] A. I. Chumakov, A. Q. Baron, I. Sergueev, C. Strohm, O. Leupold, Y. Shvyd'ko, G. V. Smirnov, R. Rüffer, Y. Inubushi, M. Yabashi, K. Tono, T. Kudo, and T. Ishikawa, Superradiance of an ensemble of nuclei excited by a free electron laser, Nature physics 14, 261 (2018).
- [36] Y. Shvyd'ko, R. Röhlsberger, O. Kocharovskaya, J. Evers, G. A. Geloni, P. Liu, D. Shu, A. Miceli, B. Stone, W. Hippler, B. Marx-Glowna, I. Uschmann, R. Loetzsch, O. Leupold, H.-C. Wille, I. Sergeev, M. Gerharz, X. Zhang, C. Grech, M. Guetg, V. Kocharyan, N. Kujala, S. Liu, W. Qin, A. Zozulya, J. Hallmann, U. Boesenberg, W. Jo, J. Möller, A. Rodriguez-Fernandez, M. Youssef, A. Madsen, and T. Kolodziej, Resonant x-ray excitation of the nuclear clock isomer ⁴⁵Sc, Nature **622**, 471–475 (2023).
- [37] P. Liu, M. Gerharz, B. Marx-Glowna, W. Hippler, J.-E. Pudell, A. Zozulya, B. Stone, D. Shu, R. Loetzsch, S. Sadashivaiah, L. Bocklage, C. Boemer, S. Liu, V. Kocharyan, D. Krebs, T. Long, W. Qin, M. Scholz, K. Schlage, I. Sergeev, H.-C. Wille, U. Boesenberg, G. A. Geloni, J. Hallmann, W. Jo, N. Kujala, A. Madsen, A. Rodriguez-Fernandez, R. Rysov, K. Tasca, T. Kolodziej, X. Zhang, M. Ilchen, N. Wieland, G. Huber, J. H. Edgar, J. Evers, O. Kocharovskaya, R. Röhlsberger, and Y. Shvyd'ko, Probing the linewidth of the 12.4-kev solid-state ⁴⁵Sc isomeric resonance (2025), arXiv:2508.17538 [quant-ph].
- [38] M. Gerharz, W. Hippler, B. Marx-Glowna, S. Sadashivaiah, K. S. Schulze, I. Uschmann, R. Lötzsch, K. Schlage, S. Velten, D. Lentrodt, L. Wolff, O. Leupold, I. Sergeev, H.-C. Wille, C. Strohm, M. Guetg, S. Liu, G. A. Geloni, U. Boesenberg, J. Hallmann, A. Zozulya, J.-E. Pudell, A. Rodriguez-Fernandez, M. Youssef, A. Madsen, L. Bocklage, G. G. Paulus, C. H. Keitel, T. Pfeifer, R. Röhlsberger, and J. Evers, Single-shot sorting of Mössbauer time-domain data at x-ray free electron lasers (2025), arXiv:2509.15833 [quant-ph].
- [39] D. Lentrodt, C. H. Keitel, and J. Evers, Toward nonlinear optics with Mössbauer nuclei using x-ray cavities, Phys. Rev. Lett. 135, 033801 (2025).
- [40] K.-J. Kim, Y. Shvyd'ko, and S. Reiche, A proposal for an x-ray free-electron laser oscillator with an energyrecovery linac, Phys. Rev. Lett. 100, 244802 (2008).
- [41] R. Margraf, R. Robles, A. Halavanau, J. Kryzywinski, K. Li, J. MacArthur, T. Osaka, A. Sakdinawat, T. Sato, Y. Sun, K. Tamasaku, Z. Huang, G. Marcus, and D. Zhu, Low-loss stable storage of 1.2 Å x-ray pulses in a 14 m bragg cavity, Nature Photonics 17, 878–882 (2023).
- [42] P. Rauer, I. Bahns, B. Friedrich, S. Casalbuoni, M. D. Felice, M. Dommach, I. F. Martin, W. Freund, J. Grünert, M. Guetg, I. Karpics, S. Karabekyan, A. Koch, N. Kujala, D. L. Civita, J. Liu, T. Maltezopoulos, M. Makita, F. Mayet, L. Müller, B. Rio, L. Samoylova, S. Schmidtchen, M. Scholz, A. Silenzi, V. Strauch, D. Thoden, T. Wohlenberg, M. Vannoni, F. Yang, W. Decking, J. Rossbach, and H. Sinn, Lasing of a cavity based x-ray source 10.21203/rs.3.rs-7274597/v1 (2025), preprint available at Research Square.
- [43] B. Adams, G. Aeppli, T. Allison, A. Q. R. Baron, P. Bucksbaum, A. I. Chumakov, C. Corder, S. P. Cramer, S. DeBeer, Y. Ding, J. Evers, J. Frisch, M. Fuchs, G. Grübel, J. B. Hastings, C. M. Heyl, L. Hol-

- berg, Z. Huang, T. Ishikawa, A. Kaldun, K.-J. Kim, T. Kolodziej, J. Krzywinski, Z. Li, W.-T. Liao, R. Lindberg, A. Madsen, T. Maxwell, G. Monaco, K. Nelson, A. Palffy, G. Porat, W. Qin, T. Raubenheimer, D. A. Reis, R. Röhlsberger, R. Santra, R. Schoenlein, V. Schünemann, O. Shpyrko, Y. Shvyd'ko, S. Shwartz, A. Singer, S. K. Sinha, M. Sutton, K. Tamasaku, H.-C. Wille, M. Yabashi, J. Ye, and D. Zhu, Scientific Opportunities with an X-ray Free-Electron Laser Oscillator (2019), arXiv:1903.09317 [physics].
- [44] C. D. Mink and M. Fleischhauer, Collective radiative interactions in the discrete truncated Wigner approximation, SciPost Phys. 15, 233 (2023).
- [45] Y. Kagan, A. M. Afanas'ev, and V. G. Kohn, On excitation of isomeric nuclear states in a crystal by synchrotron radiation, Journal of Physics C: Solid State Physics 12, 615–631 (1979).
- [46] J. P. Hannon and G. T. Trammell, Coherent γ -ray optics, Hyperfine Interactions **123**, 127 (1999).
- [47] K. P. Heeg and J. Evers, X-ray quantum optics with Mössbauer nuclei embedded in thin-film cavities, Phys. Rev. A 88, 043828 (2013).
- [48] D. Lentrodt, K. P. Heeg, C. H. Keitel, and J. Evers, Ab initio quantum models for thin-film x-ray cavity qed, Phys. Rev. Res. 2, 023396 (2020).
- [49] X. Kong, D. E. Chang, and A. Pálffy, Green's-function formalism for resonant interaction of x rays with nuclei in structured media, Phys. Rev. A 102, 033710 (2020).
- [50] D. Lentrodt, C. H. Keitel, and J. Evers, Excitation of narrow x-ray transitions in thin-film cavities by focused pulses (2025).
- [51] L. Wolff and J. Evers, Characterization and detection method for x-ray excitation of Mössbauer nuclei beyond the low-excitation regime, Phys. Rev. A 108, 043714 (2023).
- [52] K. P. Heeg, C. H. Keitel, and J. Evers, Inducing and detecting collective population inversions of Mössbauer nuclei (2016), arXiv:1607.04116 [quant-ph].
- [53] R. Röhlsberger, Nuclear Condensed Matter Physics with Synchrotron Radiation: Basic Principles, Methodology and Applications (Springer, Berlin, Heidelberg, 2004).
- [54] U. Schollwöck, The density-matrix renormalization group in the age of matrix product states, Annals of Physics 326, 96 (2011), january 2011 Special Issue.
- [55] X. Kong, Y. Chang, L. Zhang, J. Yuan, and Y.-G. Ma, Multiphoton emission of x-rays from cooperative resonant nuclei, Phys. Rev. Res. 7, 013030 (2025).
- [56] R. Kubo, Generalized cumulant expansion method, Journal of the Physical Society of Japan 17, 1100 (1962).
- [57] M. Sánchez-Barquilla, R. E. F. Silva, and J. Feist, Cumulant expansion for the treatment of light-matter interactions in arbitrary material structures, The Journal of Chemical Physics 152, 034108 (2020).
- [58] M. Kira and S. W. Koch, Cluster-expansion representation in quantum optics, Phys. Rev. A 78, 022102 (2008).
- [59] O. Rubies-Bigorda, S. Ostermann, and S. F. Yelin, Characterizing superradiant dynamics in atomic arrays via a cumulant expansion approach, Phys. Rev. Res. 5, 013091 (2023).
- [60] P. Kirton and J. Keeling, Superradiant and lasing states in driven-dissipative dicke models, New Journal of Physics 20, 015009 (2018).
- [61] S. Krämer and H. Ritsch, Generalized mean-field approach to simulate the dynamics of large open spin

- ensembles with long range interactions, The European Physical Journal D **69**, 10.1140/epjd/e2015-60266-5 (2015).
- [62] F. Robicheaux and D. A. Suresh, Beyond lowest order mean-field theory for light interacting with atom arrays, Phys. Rev. A 104, 023702 (2021).
- [63] A. Asenjo-Garcia, J. D. Hood, D. E. Chang, and H. J. Kimble, Atom-light interactions in quasi-one-dimensional nanostructures: A green's-function perspective, Phys. Rev. A 95, 033818 (2017).
- [64] Z. Ficek and S. Swain, Quantum interference and coherence: theory and experiments, Springer series in optical sciences (Springer, Heidelberg, 2005).
- [65] M. Kiffner, M. Macovei, J. Evers, and C. H. Keitel, Vacuum-induced processes in multi-level atoms, in Progress in Optics, Vol. 55 (Elsevier Science, Burlington, 2010) pp. 85–197.

- [66] L. Allen and J. Eberly, Optical resonance and two-level atoms (Dover books on physics and chemistry, 1987).
- [67] N. N. Greenwood, Mössbauer spectroscopy (Springer Science & Business Media, 2012).
- [68] O. Diekmann, D. Lentrodt, and J. Evers, Inverse design approach to x-ray quantum optics with Mössbauer nuclei in thin-film cavities, Phys. Rev. A 105, 013715 (2022).
- [69] O. Diekmann, D. Lentrodt, and J. Evers, Inverse design in nuclear quantum optics: From artificial x-ray multilevel schemes to spectral observables, Phys. Rev. A 106, 053701 (2022).
- [70] P. Longo, C. H. Keitel, and J. Evers, Tailoring superradiance to design artificial quantum systems, Scientific Reports 6, 10.1038/srep23628 (2016).
- [71] P. Longo and J. Evers, Probing few-excitation eigenstates of interacting atoms on a lattice by observing their collective light emission in the far field, Phys. Rev. A 90, 063834 (2014).